https://www.scirp.org/journal/jbise

J. Biomedical Science and Engineering, 2024, Vol. 17, (No. 11), pp: 207-217

Mechanical Behavior of Moderately Inflated Tubular Organs: A Three-Dimensional Analytical Approach

Agnès Drochon

I2M UMR CNRS 5295, Arts et Métiers Institute of Technology, University of Bordeaux, Talence, France

Correspondence to: Agnès Drochon, agnes.drochon@u-bordeaux.fr

Keywords: Tubular Organs, Inflation Experiments, Linear Elasticity, Anisotropy, Young Modulus, Poisson's Coefficients

Received: October 9, 2024 **Accepted:** November 15, 2024 **Published:** November 18, 2024

ABSTRACT

Hollow tubular tissues and organs of our body have various functions: gastrointestinal (esophagus), respiratory (trachea), and vascular (veins, arteries). A panel of pathologies is associated with each of these tissues and therapeutic interventions, surgery or replacement may be necessary. A precise knowledge of the mechanical properties of these tissues is thus required in order to understand their functioning in native conditions, to be able to elaborate some prostheses, or to design appropriate surgical training tools. These tissues may undergo expansions or contractions (peristalsis) and are exposed to internal pressures. The wall of tubular organs is organized in different layers, and each layer consists of various cell types and extra-cellular matrix, depending on the physiological functions that the organ has to fulfil. This yields anisotropic and compliant structures. In inflation experiments, the linear elasticity approach is acceptable as long as the organ's inflation remains moderate. In this paper, elasticity laws are revisited and supplemented in order to show that, coupled with modern experimental characterization tools, they provide useful information (compliances, directional Young moduli, Poisson ratios) for the design of artificial tubular organs. The importance of a precise determination of the wall thickness and its evolution during inflation is pointed out.

1. INTRODUCTION

Since the 1960s, the linear elasticity theory has been widely used to analyse inflation experiments performed with blood vessels or vascular biomaterials (a non-specialist reader can consult, for example, the resource book of Y. C. Fung [1]). Vessel walls must have enough strength in the circumferential direction to withstand arterial pressures and enough compliance to allow pulsatile flow. Classical mechanical tests consist of longitudinal or circumferential tensile tests and inflation experiments. In some studies, ultimate tensile strength, elongation at break and suture retention force are also measured. The most straightforward information deduced from inflation experiments is the compliance of the organ's wall (relative increase in diameter consecutive to a given increase in internal pressure) and the burst pressure. In order to infer more detailed mechanical parameters, a constitutive law for the wall is necessary. Linear elasticity approach is acceptable as long as the deformations remain small (corresponding to the linear part of the stress-strain curve). If the material is assumed isotropic, it is possible to infer its Young's modulus (E) and Poisson ratio (ν) from tube equilibrium equations [2]. However, the structural organization (layered microstructure composed of collagen, elastin, and SMCs (smooth muscle cells)) of vessel walls confers to them some anisotropic properties [3, 4]. Mechanical responses to some solicitations are not the same in any direction. The studies of Dobrin and Doyle [5], Dobrin [6], Lillie *et al.* [7] provide calculations for circumferential and longitudinal elastic modulus, based on the assumption that the radial stress (the stress which tends to compress the wall) amounts to only a few percents of the longitudinal and azimuthal stress. For that reason, they neglect *a priori* the σ_{rr} contribution in their analysis.

Concomitantly, mechanical tests were also performed on vascular grafts in order to check the graft patency. Some compliance mismatch between the graft and the host artery may lead to graft thrombosis [8, 9]. Dynamic compliance can be evaluated as $((D_s - D_d)/D_d)/(P_s - P_d)$ where subscripts s and d mean "systolic" and "diastolic", D is the graft diameter, and P is the internal pressure. Circumferential compliance allows the prosthesis to expand in response to the pulsatile pressure. The trend is to optimize materials and tubular bio-structures before surgery [10, 11]. Many other motivations may be cited: modeling arterial clamping or balloon dilatation, helping understand pathologies and improving treatments, fabrication of manikins for medical training or adaptation to robotic surgery.

More recently, other tubular organs have also been studied, such as esophagus or trachea. A detailed description of these organs and of their physiological functions in relation with their mechanical requirements may be found in the reviews of Pien *et al.* [4] and of Saksena *et al.* [12]. These organs may be affected by a variety of diseases or injuries: congenital malformation, autoimmune disease, inflammation, infection, and cancer. Resection and replacement are sometimes unavoidable, and may be associated with other problems (leakage, rejection, stricture). The esophagus has to be compliant enough in order to convey food to the stomach by peristalsis and contractions of the muscle layer. The trachea is submitted to air pressure variations during the respiratory cycle (inspiration/expiration). Two recent review papers are focused more precisely on the gastrointestinal tissues [13, 14]. They point out the anisotropy of these tissues due to their multi-layered structure and indicate that inflation-extension tests may be appropriate to characterize both the distension of the tissue in the circumferential direction and the stretch in the longitudinal direction.

Many groups now use tissue engineering technologies to fabricate synthetic constructs as tissue replacements for hollow tubular organs. Several review papers give an extensive description of the fabrication processes (scaffolds, cells, mechanical and biological tests required for the regenerated organ) [3, 4, 12, 15]. Mechanical and biological performances are closely linked since the scaffold stiffness influences cell-material interactions and cell differentiation. In view of implantation, anatomical accuracy, suturability, autoimmune acceptance, and long-term patency are also required for the tubular constructs. Bio-engineered tubular organs may also be used for fundamental research: basic science, a better understanding of some diseases, and drug testing. Examples of organ targeted studies may be found in De Mel *et al.* [16] (3D tubular scaffolds for paediatric organ production), Farhat *et al.* [17] (3D bioprinting for esophageal tissue repair and reconstruction), Lee *et al.* [18] (3D printing of vascularized tissues). In each case, the mechanical properties of the tubular structures are checked to match those of the human tissues.

Besides, noticeable progresses have been done with experimental characterizing tools that allow three-dimensional measurements of local strains and stresses. Bernal *et al.* [19] proposed a technique that uses sonometry data from piezoelectric elements to measure the strain in the longitudinal and circumferential directions of pressurized arteries. A review by Macrae *et al.* [20] is especially dedicated to "methods in mechanical testing of arterial tissues". In addition to improved optical measuring systems, marker tracking, CT scan or electronic speckle pattern interferometry are quoted as techniques that allow to evaluate stresses and strains. Sanders *et al.* [21] used ultrasound strain imaging in whole-vessel-inflation experiments. Strain maps were obtained through intravascular ultrasound elastography. They aimed at characterizing mechanical properties of the different atherosclerotic plaque constituents in order to evaluate the rupture risk of the plaque. An optical clearing method is adopted by Maeda *et al.* [22]. It is coupled with imaging and microscopy techniques and allows some three-dimensional characterization of the mechanical behavior of rat thoracic aorta under intraluminal pressurization. Microstructural analysis of the inflated tissue is provided. Urban *et al.* [23] demonstrate that the ultra-sound technique can be precise enough to capture the diameter variation of an artery due to the pressure pulse transmitted by blood flow. This allows to evaluate the compliance of the artery wall. In future works, they plan to use different US propagating modes in the axial and circumferential directions in order to capture anisotropic mechanical properties of the vessel wall.

In this context, elasticity laws are revisited and completed in this paper. If coupled with microstructural measurements provided by modern experimental tools, the proposed three-dimensional analysis of the deformation of anisotropic tubular organs under moderate inflation can allow a more detailed comprehension of the mechanical behavior of native and fabricated tissues.

2. THEORETICAL METHODOLOGY

Let us consider a hollow tubular organ with the following known initial dimensions: wall thickness h_0, external diameter d_{e0}, ($d_{e0} = 2r_{e0}$), length l_0. Classical cylindrical coordinates (r, θ, z) are used, and z is the longitudinal axis (**Figure 1**). If an internal pressure P is applied inside the tube (the external pressure is taken as zero), its diameter will increase due to the compliance of the wall.

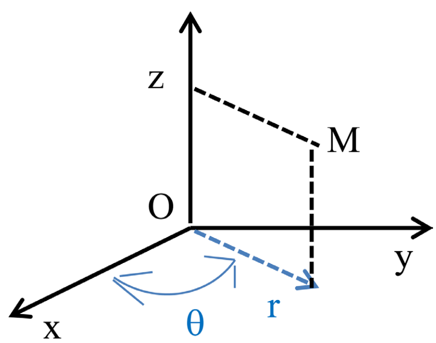

Figure 1. Cylindrical coordinates.

This increase in diameter is associated with a decrease in wall thickness and a length variation. The dimensions in the deformed state are denoted h for the wall thickness, d_e (= $2r_e$) for the diameter, and l for the length. (**Figure 2**)

The internal radii at time $t = 0$ are easily obtained as:

$$r_{i0} = r_{e0} - h_0 \tag{1}$$

The initial cross section of the esophagus wall is:

$$S_0 = \pi\left(r_{e0}^2 - r_{i0}^2\right) \tag{2}$$

Wall incompressibility [24, 25] yields:

$$\pi\left(r_e^2 - r_i^2\right)l = \pi\left(r_{e0}^2 - r_{i0}^2\right)l_0 \tag{3}$$

The deformed internal radius r_i is deduced from this wall volume conservation. Then, the deformed wall thickness, h, may be evaluated as:

$$h = r_e - r_i \tag{4}$$

The initial volume of the esophagus is:

$$V_0 = \pi r_{e0}^2 l_0 \tag{5}$$

and its volume in the inflated state is:

$$V = \pi r_e^2 l \tag{6}$$

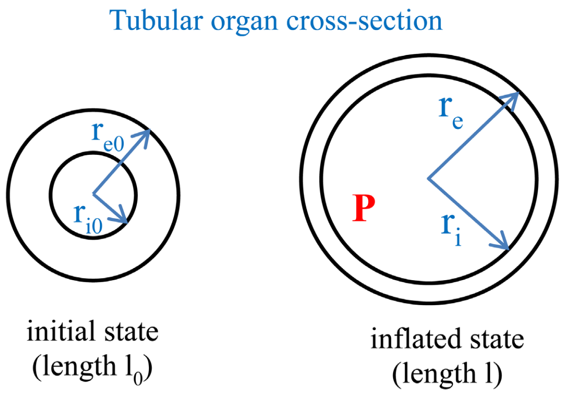

Figure 2. Tubular organ geometry in the initial state and under internal pressure *P*.

This allows to calculate a compliance, based on the relative volume variation in response to the imposed internal pressure *P*:

$$C_v = \frac{\left(\frac{V - V_0}{V_0}\right)}{P} \tag{7}$$

The inverse of C_v ($E_p = 1/C_v$) may be interpreted as a "pressure elastic modulus". A compliance based on diameter variation, C_d, may also be defined:

$$C_d = \frac{\left(\frac{d_e - d_{e0}}{d_{e0}}\right)}{P} \tag{8}$$

However, these compliances C_d and C_v do not account for the changes in wall thickness [26]. A possible length variation during inflation is taken into account in C_v, but not in C_d.

A three-dimensional analysis may be proposed as follows:

Classical notations in a cylindrical frame are used for the extension ratios: $\lambda_z = l/l_0$ is the longitudinal extension ratio; $\lambda_\theta = d_e/d_{e0}$ is the circumferential extension ratio (perimeter of the inflated tube/perimeter of the initial tube) and $\lambda_r = h/h_0$ is the radial stretch ratio (change of dimension in the radial direction). As explained by Patel *et al.* [27] and Dobrin and Doyle [5], only orthogonal elongating strains in the three principal geometric directions need to be considered when the tubular sample is loaded by inflation and longitudinal traction.

The corresponding deformations are denoted e_{rr}, $e_{\theta\theta}$, and e_{zz}, with

$$e_{rr} = \lambda_r - 1,\ e_{\theta\theta} = \lambda_\theta - 1,\ e_{zz} = \lambda_z - 1 \tag{9}$$

We adopt the following approached formulas in order to compute the stresses in the esophagus wall:

- The radial normal stress, σ_{rr}, is estimated as:

$$\sigma_{rr} = -P/2 \tag{10}$$

(This is the mean value between the internal pressure P, and the external pressure (0)).
- The circumferential stress, $\sigma_{\theta\theta}$, is:

$$\sigma_{\theta\theta} = P\frac{r_i}{h} \tag{11}$$

The longitudinal stress, σ_{zz}, is calculated as the sum of two components:

$$\sigma_{zz} = \frac{P\pi r_i^2}{\pi\left(r_e^2 - r_i^2\right)} + \sigma_{zext} \tag{12}$$

where the first term corresponds to the longitudinal stress due to pressure and the second term (σ_{zext}) is the stress due to an eventual external longitudinally applied traction.

These formulas have been widely used for inflated elastic tissues (for example, blood vessels) [5-7, 27]. They rely on the assumption that the wall thickness h is small when compared to the vessel radius r, and that σ_{rr} varies linearly across the wall. They were initially deduced from the equations describing the equilibrium of an isotropic inflated elastic tube, that are recalled in [10]. As explained above, in such inflation experiments, shear stresses and shear deformations are classically neglected [19].

Constitutive equations for static anisotropic elasticity may be derived from the paper of Patel *et al.* [27]:

$$\begin{pmatrix} e_{rr} \\ e_{\theta\theta} \\ e_{zz} \end{pmatrix} = \begin{pmatrix} \frac{1}{E_r} & -\frac{\nu_{r\theta}}{E_\theta} & -\frac{\nu_{rz}}{E_z} \\ -\frac{\nu_{\theta r}}{E_r} & \frac{1}{E_\theta} & -\frac{\nu_{\theta z}}{E_z} \\ -\frac{\nu_{zr}}{E_r} & -\frac{\nu_{z\theta}}{E_\theta} & \frac{1}{E_z} \end{pmatrix} \begin{pmatrix} \sigma_{rr} \\ \sigma_{\theta\theta} \\ \sigma_{zz} \end{pmatrix} \tag{13}$$

where E_r (Pa), E_θ (Pa) and E_z (Pa) denote the elastic moduli in the radial, circumferential and longitudinal directions.

Due to symmetry conditions, some additional relations exist:

$$\frac{\nu_{z\theta}}{E_\theta} = \frac{\nu_{\theta z}}{E_z}\ ;\ \frac{\nu_{zr}}{E_r} = \frac{\nu_{rz}}{E_z}\ ;\ \frac{\nu_{r\theta}}{E_\theta} = \frac{\nu_{\theta r}}{E_r} \tag{14}$$

The quantities $\nu_{r\theta}$, ν_{rz}, $\nu_{\theta z}$, $\nu_{\theta r}$, ν_{zr}, $\nu_{z\theta}$ are Poisson ratios. For example, $\nu_{r\theta}$ represents the ratio of the contractile strain in the radial direction due to an elongating strain in the circumferential direction, ν_{rz} represents the ratio of the contractile strain in the radial direction due to an elongating strain in the longitudinal direction, etc. More generally, ν_{ij} characterize the strain in the i-direction produced by a loading in the j-direction.

The incompressibility of the tissue imposes the following condition:

$$e_{rr} + e_{\theta\theta} + e_{zz} = 0 \tag{15}$$

The condition (15) may be expressed using Equation (13).
This writes:

$$\frac{\sigma_{rr}}{E_r} - \frac{\nu_{r\theta}}{E_\theta}\sigma_{\theta\theta} - \frac{\nu_{rz}}{E_z}\sigma_{zz} - \frac{\nu_{\theta r}}{E_r}\sigma_{rr} + \frac{\sigma_{\theta\theta}}{E_\theta} - \frac{\nu_{\theta z}}{E_z}\sigma_{zz} - \frac{\nu_{zr}}{E_r}\sigma_{rr} - \frac{\nu_{z\theta}}{E_\theta}\sigma_{\theta\theta} + \frac{\sigma_{zz}}{E_z} = 0 \tag{16}$$

that is:

$$\frac{\sigma_{rr}}{E_r}\left(1 - \nu_{\theta r} - \nu_{zr}\right) + \frac{\sigma_{\theta\theta}}{E_\theta}\left(1 - \nu_{r\theta} - \nu_{z\theta}\right) + \frac{\sigma_{zz}}{E_z}\left(1 - \nu_{rz} - \nu_{\theta z}\right) = 0 \tag{17}$$

In order that Equation (17) can be satisfied in any case, the factor of σ_{rr}/E_r in this sum has to be null, idem for the factor of $\sigma_{\theta\theta}/E_\theta$, and the factor of σ_{zz}/E_z. Consequently,

$$\begin{cases} \nu_{\theta r} + \nu_{zr} = 1 \\ \nu_{r\theta} + \nu_{z\theta} = 1 \\ \nu_{rz} + \nu_{\theta z} = 1 \end{cases} \tag{18}$$

or equivalently (using (14)):

$$\begin{cases} \nu_{r\theta}\dfrac{E_r}{E_\theta} + \nu_{rz}\dfrac{E_r}{E_z} = 1 \\ \nu_{r\theta} + \nu_{\theta z}\dfrac{E_\theta}{E_z} = 1 \\ \nu_{rz} + \nu_{\theta z} = 1 \end{cases} \tag{19}$$

The Poisson coefficients $\nu_{r\theta}$, ν_{rz}, and $\nu_{\theta z}$ thus depend on the orthogonal elastic moduli and may be deduced from the system of Equation (19):

$$\nu_{rz} = \frac{1}{2} - \frac{1}{2}E_z\left(\frac{1}{E_\theta} - \frac{1}{E_r}\right) \tag{20}$$

$$\nu_{r\theta} = \frac{1}{2} - \frac{1}{2}E_\theta\left(\frac{1}{E_z} - \frac{1}{E_r}\right) \tag{21}$$

$$\nu_{\theta z} = \frac{1}{2} - \frac{1}{2}E_z\left(\frac{1}{E_r} - \frac{1}{E_\theta}\right) \tag{22}$$

and then

$$\nu_{\theta r} = \frac{1}{2} - \frac{1}{2}E_r\left(\frac{1}{E_z} - \frac{1}{E_\theta}\right) \tag{23}$$

$$\nu_{zr} = \frac{1}{2} - \frac{1}{2}E_r\left(\frac{1}{E_\theta} - \frac{1}{E_z}\right) \tag{24}$$

$$\nu_{z\theta} = \frac{1}{2} - \frac{1}{2}E_\theta\left(\frac{1}{E_r} - \frac{1}{E_z}\right) \tag{25}$$

One can notice that:

$$\frac{1}{6}\left(\nu_{r\theta} + \nu_{rz} + \nu_{\theta z} + \nu_{\theta r} + \nu_{zr} + \nu_{z\theta}\right) = \frac{1}{2} \tag{26}$$

and that Equation (22) is also given in Lillie *et al.* [7], with the physical meaning of "a decrease in radius obtained on the increase in length under uniaxial load". Equations (20) to (25) thus develop and confirm the approach initiated by Patel *et al.* [27].

In the case of isotropy $E_r = E_\theta = E_z$ and, as expected for an incompressible material,

$$\nu_{r\theta} = \nu_{rz} = \nu_{\theta z} = \nu_{\theta r} = \nu_{zr} = \nu_{z\theta} = \frac{1}{2}.$$

Equation (13) coupled with Equations (20) to (25) can be re-written as follows:

$$\begin{cases} e_{rr} = \frac{1}{E_r}\sigma_{rr} - \sigma_{\theta\theta}\left(\frac{1}{2E_\theta} - \frac{1}{2E_z} + \frac{1}{2E_r}\right) - \sigma_{zz}\left(\frac{1}{2E_z} - \frac{1}{2E_\theta} + \frac{1}{2E_r}\right) \\ e_{\theta\theta} = -\sigma_{rr}\left(\frac{1}{2E_\theta} - \frac{1}{2E_z} + \frac{1}{2E_r}\right) + \frac{1}{E_\theta}\sigma_{\theta\theta} - \sigma_{zz}\left(\frac{1}{2E_z} - \frac{1}{2E_r} + \frac{1}{2E_\theta}\right) \\ e_{zz} = -\sigma_{rr}\left(\frac{1}{2E_z} - \frac{1}{2E_\theta} + \frac{1}{2E_r}\right) - \sigma_{\theta\theta}\left(\frac{1}{2E_z} - \frac{1}{2E_r} + \frac{1}{2E_\theta}\right) + \frac{1}{E_z}\sigma_{zz} \end{cases} \tag{27}$$

The relative deformations e_{rr}, $e_{\theta\theta}$, e_{zz} can be deduced from the experiments (Equation (9)); the normal stresses σ_{rr}, $\sigma_{\theta\theta}$, and σ_{zz} can be estimated using Equations (10) to (12).

One may introduce the quantities: $X_r = 1/E_r$, $X_\theta = 1/E_\theta$, and $X_z = 1/E_z$. The system to solve thus becomes:

$$\begin{cases} 2e_{rr} = X_r(2\sigma_{rr} - \sigma_{\theta\theta} - \sigma_{zz}) + (\sigma_{zz} - \sigma_{\theta\theta})X_\theta - (\sigma_{zz} - \sigma_{\theta\theta})X_z \\ 2e_{\theta\theta} = (\sigma_{zz} - \sigma_{rr})X_r + X_\theta(-\sigma_{rr} + 2\sigma_{\theta\theta} - \sigma_{zz}) - (\sigma_{zz} - \sigma_{rr})X_z \\ 2e_{zz} = -(\sigma_{rr} - \sigma_{\theta\theta})X_r + (\sigma_{rr} - \sigma_{\theta\theta})X_\theta + X_z(-\sigma_{rr} - \sigma_{\theta\theta} + 2\sigma_{zz}) \end{cases} \tag{28}$$

Since the 3 equations of this system are linked by the relation: $e_{rr} + e_{\theta\theta} + e_{zz} = 0$, one of the unknown has to be taken as a parameter or determined by another method (for example, traction experiments performed with the studied tissue samples). If we suppose that the longitudinal modulus, E_z, is known, X_r and X_θ are deduced from Equation (28) and expressed as functions of e_{rr}, $e_{\theta\theta}$, and X_z.

$$X_r = \frac{1}{E_r} = e_{rr}\frac{\sigma_{rr} - 2\sigma_{\theta\theta} + \sigma_{zz}}{(\sigma_{rr} - \sigma_{\theta\theta})^2} + e_{\theta\theta}\frac{\sigma_{zz} - \sigma_{\theta\theta}}{(\sigma_{rr} - \sigma_{\theta\theta})^2} + X_z\frac{(\sigma_{zz} - \sigma_{\theta\theta})^2}{(\sigma_{rr} - \sigma_{\theta\theta})^2} \tag{29}$$

$$X_\theta = \frac{1}{E_\theta} = e_{rr}\frac{\sigma_{zz} - \sigma_{rr}}{(\sigma_{rr} - \sigma_{\theta\theta})^2} - e_{\theta\theta}\frac{2\sigma_{rr} - \sigma_{\theta\theta} - \sigma_{zz}}{(\sigma_{rr} - \sigma_{\theta\theta})^2} + X_z\frac{(\sigma_{rr} - \sigma_{zz})^2}{(\sigma_{rr} - \sigma_{\theta\theta})^2} \tag{30}$$

Coming back to Equation (20) to (25), it is then possible to calculate all the Poisson coefficients.

3. ILLUSTRATIVE EXAMPLE WITH LITERATURE DATA

Intraluminal pressurization of rat thoracic aorta is considered. The data are taken from Maeda *et al.* [22]. The specimen initial geometry is h_0 = 150 µm, r_{e0} = 1 mm, l_0 = 20 mm (so that the initial internal radius r_{i0} = 0.85 mm). For an internal pressure P = 40 mmHg, the deformations $e_{\theta\theta}$ and e_{zz} are reported as: $e_{\theta\theta}$ = 0.26 and e_{zz} = 0.008. It is thus possible to calculate the deformed geometry: r_e = 1.26 mm, r_i = 1.146 mm, h = 114.3 µm. These geometric data are summarized in Table 1.

Table 1. Specimen geometry (Ref. [22] is the data source).

	Internal radius r_i (mm)	External radius r_e (mm)	Thickness (µm)	Length (mm)
Before inflation	0.85	1	150	20
Inflated	1.146	1.26	114.3	20.16

Table 2. Stresses calculated with measurements from [22].

σ_{rr} (Pa)	$\sigma_{\theta\theta}$ (Pa)	σ_{zz} (Pa)
−2667	0.534×10^5	0.254×10^5

Table 3. Young moduli calculated with measurements from [22].

E_r (Pa)	E_θ (Pa)	E_z (Pa) (from [25])
1.53×10^5	1.36×10^5	1×10^5

Table 4. Poisson coefficients calculated with measurements from [22].

ν_{rz}	$\nu_{r\theta}$	$\nu_{\theta z}$	$\nu_{\theta r}$	ν_{zr}	$\nu_{z\theta}$
0.459	0.264	0.54	0.296	0.7	0.736

The volume compliance (Equation (7)) is 1.12×10^{-4} Pa^{-1} and the diameter compliance (Equation (8)) is 4.87×10^{-5} Pa^{-1}. The radial stretch ratio λ_r is 0.762 so that $e_{rr} = -0.238$. The stresses are obtained through Equations (10)-(12) and are summarized in **Table 2**. It is observed that, as expected, $\sigma_{\theta\theta} \approx 2\sigma_{zz}$. The radial stress (the stress which tends to compress the wall) amounts to only 10 % of the longitudinal stress and 5% of the azimuthal stress. For that reason, some authors [5, 7, 28] neglect *a priori* the σ_{rr} contribution in their analysis. Using the value of Assoul *et al.* [25] for the longitudinal elastic modulus E_z of the rat thoracic aorta ($E_z = 1 \times 10^5$ Pa), the radial and circumferential elastic moduli are deduced from Equation (29) and (30): $E_r = 1.53 \times 10^5$ Pa, and $E_\theta = 1.36 \times 10^5$ Pa. These results are summarized in **Table 3**. The corresponding Poisson coefficients (Equations (20)-(25)) are presented in **Table 4**.

No sophisticated interpretation of these results can be made because they are based on rough estimations of the input data. However, the orders of magnitude are in good agreement with similar results that can be found in the literature. Cox [29] studied the anisotropic properties of the canine carotid artery with significant axial pre-stress ($\lambda_z > 1.5$) and pressures up to 200 mmHg. He mentions that the elastic moduli (in the range 10^5 - 10^6 Pa) and the various Poisson ratios (between 0 and 1) are complex functions of the extension ratios. For the elastic moduli of aortas (estimated in living dogs), Patel *et al.* [27] report values in the range 3.9×10^5 Pa to 8.8×10^5 Pa, with $E_r < E_\theta$ and E_z, depending on the extension ratio values (λ_θ and λ_z varying between 1.4 and 1.6). Nahon *et al.* [28] examined the mechanical properties of canine iliac arteries under operating pressures of 80 to 160 mmHg. Their approach is two-dimensional. For an internal pressure of 80 mmHg, they obtain $E_\theta = 2 \times 10^5$ Pa, $E_z = 4.6 \times 10^5$ Pa and $\nu_{\theta z} = 0.56$. They also indicate a compliance value of 2.25×10^{-5} Pa^{-1} for some canine femoral artery. More recently, an attempt was made by Sugita *et al.* [30] to evaluate 3D local strains (at the cell scale) in mice thoracic aortas during intraluminal pressurization. In their work, one can also find an estimation of the volume compliance of the studied vessels around 0.37×10^{-4} Pa^{-1}. Skacel and Bursa [31] tried to establish some relations between the Poisson ratios and the internal layered structure of the arteries walls. Their demonstration is based on uniaxial traction experiments of porcine aortic wall. They show that "in-plane" Poisson ratios are between 0 and 0.5 and "out-of-plane" Poisson ratios can get values between 0.5 and 1. They also point out the importance of the transversal contraction (in the thickness direction).

4. DISCUSSION

i) It may be of interest to evaluate if the assumption of isotropy in the analysis of inflation experiments would yield very different results. If the mechanical properties are supposed to be identical in all directions, the incompressibility condition leads to a value of 0.5 for ν, and the Young's modulus may be found in Bergel [2]:

$$E_B = \frac{\Delta P}{\left(\frac{\Delta r_e}{r_{e0}}\right)} \frac{2\left(1-\nu^2\right) r_i^2}{r_e^2 - r_i^2} \tag{31}$$

This equation is established with the hypothesis that no change in length occurs during the inflation experiment. Since $\nu = 0.5$, Equation (31) becomes:

$$E_B = \frac{\Delta P}{\left(\dfrac{\Delta r_e}{r_{e0}}\right)} \frac{3r_i^2}{2\left(r_e^2 - r_i^2\right)} \tag{32}$$

A change in length Δl may be easily taken into account as a boundary condition in the longitudinal displacement. This leads to the following formula for the elastic modulus:

$$E_{Bmodified} = \frac{\Delta P}{\dfrac{\Delta r_e}{r_{e0}} + \nu \dfrac{\Delta l}{l_0}} \frac{2\left(1-\nu^2\right) r_i^2}{r_e^2 - r_i^2} \tag{33}$$

One can notice that if $\Delta l = 0$, Equation (33) reduces to Equation (31). Using the notations of this paper, $\Delta P = P\text{-}0$, $\Delta r_e / r_{e0} = e_{\theta\theta}$, and $\Delta l / l_0 = e_{zz}$.

The E_B modulus as defined in Equation (31) may be closely related to a circumferential modulus, since it is inversely proportional to the wall compliance C_d (Equation (8)) and proportional to a geometric factor of order (r_i/h):

$$E_B = \frac{1}{C_d} \frac{2\left(1-\nu^2\right) r_i^2}{\left(r_e - r_i\right)\left(r_e + r_i\right)} \approx \frac{1}{C_d} \frac{\left(1-\nu^2\right) r_i}{h} \tag{34}$$

With the numerical data adopted in Section 3, the value of E_B from Equation (32) is 1.47×10^5 Pa and the value from Equation (34) is 1.54×10^5 Pa. Both values are close to the E_θ value obtained in Section 3 ($E_\theta = 1.36 \times 10^5$ Pa).

ii) If internal pressures and tube radii are increased further, the linear elasticity approach is no longer valid. The stiffness of the tissue increases with the load, and this produces an exponential stress-strain relationship. Different models have been proposed in the literature to describe this hyperelastic behavior. One of the most popular is the "HGO-model" [32].

5. CONCLUSION

In spite of the simplifying hypotheses that are made, the theoretical approaches presented in this paper may be useful for the interpretation of inflation experiments of tubular elastic biological tissues. Inflation induces deformations of the organ's wall in three directions (radial, circumferential, and longitudinal). Each deformation influences the two others. The Poisson ratios are the physical quantities that put in evidence of this coupling. This paper stresses the importance of analyzing the evolution of the wall thickness during inflation and suggests the possibility of combining mechanical results with very detailed microscopic or imaging results.

CONFLICTS OF INTEREST

The author declares no conflicts of interest regarding the publication of this paper.

REFERENCES

1. Fung, Y.C. (1993) Biomechanics: Mechanical Properties of Living Tissues. 2nd Edition, Springer.
2. Bergel, D.H. (1961) The Static Elastic Properties of the Arterial Wall. *The Journal of Physiology*, **156**, 445-457. https://doi.org/10.1113/jphysiol.1961.sp006686
3. Boys, A.J., Barron, S.L., Tilev, D. and Owens, R.M. (2020) Building Scaffolds for Tubular Tissue Engineering.

Frontiers in Bioengineering and Biotechnology, **8**, Article ID: 589960. https://doi.org/10.3389/fbioe.2020.589960

4. Pien, N., Palladino, S., Copes, F., Candiani, G., Dubruel, P., Van Vlierberghe, S., *et al.* (2021) Tubular Bioartificial Organs: From Physiological Requirements to Fabrication Processes and Resulting Properties. A Critical Review. *Cells Tissues Organs*, **211**, 420-446. https://doi.org/10.1159/000519207
5. Dobrin, P.B. and Doyle, J.M. (1970) Vascular Smooth Muscle and the Anisotropy of Dog Carotid Artery. *Circulation Research*, **27**, 105-119. https://doi.org/10.1161/01.res.27.1.105
6. Dobrin, P.B. (1986) Biaxial Anisotropy of Dog Carotid Artery: Estimation of Circumferential Elastic Modulus. *Journal of Biomechanics*, **19**, 351-358. https://doi.org/10.1016/0021-9290(86)90011-4
7. Lillie, M.A., Shadwick, R.E. and Gosline, J.M. (2010) Mechanical Anisotropy of Inflated Elastic Tissue from the Pig Aorta. *Journal of Biomechanics*, **43**, 2070-2078. https://doi.org/10.1016/j.jbiomech.2010.04.014
8. Abbott, W.M., Megerman, J., Hasson, J.E., L'Italien, G. and Warnock, D.F. (1987) Effect of Compliance Mismatch on Vascular Graft Patency. *Journal of Vascular Surgery*, **5**, 376-382. https://doi.org/10.1016/0741-5214(87)90148-0
9. Li, C., Wang, F., Douglas, G., Zhang, Z., Guidoin, R. and Wang, L. (2017) Comprehensive Mechanical Characterization of PLA Fabric Combined with PCL to Form a Composite Structure Vascular Graft. *Journal of the Mechanical Behavior of Biomedical Materials*, **69**, 39-49. https://doi.org/10.1016/j.jmbbm.2016.11.005
10. Castillo-Cruz, O., Pérez-Aranda, C., Gamboa, F., Cauich-Rodríguez, J.V., Mantovani, D. and Avilés, F. (2018) Prediction of Circumferential Compliance and Burst Strength of Polymeric Vascular Grafts. *Journal of the Mechanical Behavior of Biomedical Materials*, **79**, 332-340. https://doi.org/10.1016/j.jmbbm.2017.12.031
11. Camasão, D.B. and Mantovani, D. (2021) The Mechanical Characterization of Blood Vessels and Their Substitutes in the Continuous Quest for Physiological-Relevant Performances. A Critical Review. *Materials Today Bio*, **10**, Article ID: 100106. https://doi.org/10.1016/j.mtbio.2021.100106
12. Saksena, R., Gao, C., Wicox, M. and de Mel, A. (2016) Tubular Organ Epithelialisation. *Journal of Tissue Engineering*, **7**. https://doi.org/10.1177/2041731416683950
13. Patel, B., Gizzi, A., Hashemi, J., Awakeem, Y., Gregersen, H. and Kassab, G. (2022) Biomechanical Constitutive Modeling of the Gastrointestinal Tissues: A Systematic Review. *Materials & Design*, **217**, Article ID: 110576. https://doi.org/10.1016/j.matdes.2022.110576
14. Durcan, C., Hossain, M., Chagnon, G., Perić, D. and Girard, E. (2023) Mechanical Experimentation of the Gastrointestinal Tract: A Systematic Review. *Biomechanics and Modeling in Mechanobiology*, **23**, 23-59. https://doi.org/10.1007/s10237-023-01773-8
15. Jeong, H., Nam, H., Jang, J. and Lee, S. (2020) 3D Bioprinting Strategies for the Regeneration of Functional Tubular Tissues and Organs. *Bioengineering*, **7**, Article No. 32. https://doi.org/10.3390/bioengineering7020032
16. de Mel, A., Yap, T., Cittadella, G., Hale, L.R., Maghsoudlou, P., de Coppi, P., *et al.* (2015) A Potential Platform for Developing 3D Tubular Scaffolds for Paediatric Organ Development. *Journal of Materials Science*: *Materials in Medicine*, **26**, Article No. 141. https://doi.org/10.1007/s10856-015-5477-4
17. Farhat, W., Chatelain, F., Marret, A., Faivre, L., Arakelian, L., Cattan, P., *et al.* (2021) Trends in 3D Bioprinting for Esophageal Tissue Repair and Reconstruction. *Biomaterials*, **267**, Article ID: 120465. https://doi.org/10.1016/j.biomaterials.2020.120465
18. Lee, H., Jang, T., Han, G., Kim, H. and Jung, H. (2021) Freeform 3D Printing of Vascularized Tissues: Challenges and Strategies. *Journal of Tissue Engineering*, **12**. https://doi.org/10.1177/20417314211057236
19. Bernal, M., Urban, M.W., Rosario, D., Aquino, W. and Greenleaf, J.F. (2011) Measurement of Biaxial Mechanical Properties of Soft Tubes and Arteries Using Piezoelectric Elements and Sonometry. *Physics in Medicine and Biology*, **56**, 3371-3386. https://doi.org/10.1088/0031-9155/56/11/012

20. Macrae, R.A., Miller, K. and Doyle, B.J. (2016) Methods in Mechanical Testing of Arterial Tissue: A Review. *Strain*, **52**, 380-399. https://doi.org/10.1111/str.12183

21. Sanders, S.N., Lopata, R.G.P., van Breemen, L.C.A., van de Vosse, F.N. and Rutten, M.C.M. (2020) A Novel Technique for the Assessment of Mechanical Properties of Vascular Tissue. *Biomechanics and Modeling in Mechanobiology*, **19**, 1585-1594. https://doi.org/10.1007/s10237-020-01292-w

22. Maeda, E., Ando, Y., Takeshita, K. and Matsumoto, T. (2022) Through the Cleared Aorta: Three-Dimensional Characterization of Mechanical Behaviors of Rat Thoracic Aorta under Intraluminal Pressurization Using Optical Clearing Method. *Scientific Reports*, **12**, Article No. 8632. https://doi.org/10.1038/s41598-022-12429-5

23. Urban, M.W. (2023) Understanding Arterial Biomechanics with Ultrasound and Waveguide Models. *Acoustics Today*, **19**, 46-54. https://doi.org/10.1121/at.2023.19.1.46

24. Sommer, G., Schriefl, A., Zeindlinger, G., Katzensteiner, A., Ainödhofer, H., Saxena, A., *et al*. (2013) Multiaxial Mechanical Response and Constitutive Modeling of Esophageal Tissues: Impact on Esophageal Tissue Engineering. *Acta Biomaterialia*, **9**, 9379-9391. https://doi.org/10.1016/j.actbio.2013.07.041

25. Assoul, N., Flaud, P., Chaouat, M., Letourneur, D. and Bataille, I. (2008) Mechanical Properties of Rat Thoracic and Abdominal Aortas. *Journal of Biomechanics*, **41**, 2227-2236. https://doi.org/10.1016/j.jbiomech.2008.04.017

26. Takeda, T., Kassab, G., Liu, J., Puckett, J.L., Mittal, R.R. and Mittal, R.K. (2002) A Novel Ultrasound Technique to Study the Biomechanics of the Human Esophagus *in Vivo*. *American Journal of Physiology-Gastrointestinal and Liver Physiology*, **282**, G785-G793. https://doi.org/10.1152/ajpgi.00394.2001

27. Patel, D.J., Janicki, J.S. and Carew, T.E. (1969) Static Anisotropic Elastic Properties of the Aorta in Living Dogs. *Circulation Research*, **25**, 765-779. https://doi.org/10.1161/01.res.25.6.765

28. Nahon, D., Lee, J.M. and Wilson, G.J. (1986) A Two-Dimensional Incremental Study of the Static Mechanical Properties of Vascular Grafts. *Clinical Materials*, **1**, 177-197. https://doi.org/10.1016/s0267-6605(86)80031-2

29. Cox, R.H. (1975) Anisotropic Properties of the Canine Carotid Artery in Vitro. *Journal of Biomechanics*, **8**, 293-300. https://doi.org/10.1016/0021-9290(75)90081-0

30. Sugita, S., Kato, M., Wataru, F. and Nakamura, M. (2019) Three-Dimensional Analysis of the Thoracic Aorta Microscopic Deformation during Intraluminal Pressurization. *Biomechanics and Modeling in Mechanobiology*, **19**, 147-157. https://doi.org/10.1007/s10237-019-01201-w

31. Skacel, P. and Bursa, J. (2022) Poisson's Ratio and Compressibility of Arterial Wall—Improved Experimental Data Reject Auxetic Behaviour. *Journal of the Mechanical Behavior of Biomedical Materials*, **131**, Article ID: 105229. https://doi.org/10.1016/j.jmbbm.2022.105229

32. Holzapfel, G.A., Gasser, T.C. and Ogden, R.W. (2000) A New Constitutive Framework for Arterial Wall Mechanics and a Comparative Study of Material Models. *Journal of Elasticity and the Physical Science of Solids*, **61**, 1-48. https://doi.org/10.1023/a:1010835316564